CROSS SECTION ASYMMETRY OF THE $^{12}C(\vec{\gamma}, p_0)^{11}B$ AND $^{12}C(\vec{\gamma}, p_1)^{11}B$ REACTIONS AT PHOTON ENERGIES $40...55\,MeV$

***D. D. Burdeinyi*[1], *J. Brudvik*[2], *V. B. Ganenko*[1*], *K. Hansen*[3], *K. Fissum*[3], *K. Livingston*[4], *L. Isaksson*[2], *M. Lundin*[2], *B. Nilsson*[2], *B. Schröder*[2,3]**

[1] *National Science Center "Kharkiv Institute of Physics and Technology", 61108 Kharkiv, Ukraine;*

[2] *MAX-lab, Lund University, SE-221 00 Lund, Sweden;*

[3] *Department of Physics, Lund University, SE-221 00 Lund, Sweden;*

[4] *Department of Physics and Astronomy, University of Glasgow, Glasgow G12 8QQ, Scotland, UK*

(Received July 10, 2018)

The asymmetry of the cross section of the $^{12}C(\vec{\gamma}, p_0)^{11}B$ and $^{12}C(\vec{\gamma}, p_1)^{11}B$ reactions has been measured in the energy range $40...55\,MeV$ using linearly polarized tagged photons of the MAX-lab facility. The asymmetry of the process $^{12}C(\vec{\gamma}, p_0)^{11}B$ is $\Sigma \approx 0.85$, that implies one-particle reaction mechanism. The asymmetry of the reaction $^{12}C(\vec{\gamma}, p_1)^{11}B$ is smaller, $\Sigma \approx 0.6...0.7$, that may be due to the stronger relative contribution of the $2h-1p$ mechanism to the dominant one-particle reaction mechanism.

PACS: 03.65.Pm, 03.65.Ge, 61.80.Mk

1. INTRODUCTION

In a previous paper [1], the preliminary results of measuring the cross section asymmetry of the carbon disintegration reactions $^{12}C(\vec{\gamma}, p_{01})^{11}B$ and $^{12}C(\vec{\gamma}, p_{2-6})^{11}B$ have been presented. The cross section asymmetry is defined as,

$$\Sigma = \frac{d\sigma_{\parallel} - d\sigma_{\perp}}{d\sigma_{\parallel} + d\sigma_{\perp}}, \qquad (1)$$

where $d\sigma_{\parallel(\perp)} \equiv d\sigma_{\parallel(\perp)}/d\Omega$ is the reaction cross section for the photon polarization direction parallel (perpendicular) to the reaction plane. The measurements have been produced at the MAX-lab Nuclear Physics facility in the photon energy range $E_\gamma \sim 40...55\,MeV$, using the tagged linearly polarized photon beam [2, 3]. In the experiment, the protons were detected by an available $\Delta E - E$ telescope (CsI/SSD), which was not optimized for for measurements of the $(\vec{\gamma}, p)$ reactions with a high energy resolution. It consisted of two rather thick silicon strip detectors (SSDs), each of $0.5\,mm$ thick, and a CsI(Tl) counter, and provided the energy resolution of the missing energy spectra $\sim 3...3.5\,MeV$ (FWHM) that did not allowed to resolve the final states of the ^{11}B nucleus. Therefore, the cross sections asymmetry was measured for reactions corresponding to the two groups of states of the ^{11}B nucleus: the reaction $^{12}C(\vec{\gamma}, p_{01})^{11}B$ for the ground and the first excited states of the ^{11}B, and the reaction $^{12}C(\vec{\gamma}, p_{2-6})^{11}B$ resulting from group of states producing a maximum at $E_{ex} \approx 6\,$MeV.

The measurements [1] has shown that asymmetry of the $^{12}C(\vec{\gamma}, p_{01})^{11}B$ reaction is rather high, $\Sigma \approx 0.8$, and is determined, in all probability, by the dominant $^{12}C(\vec{\gamma}, p_0)^{11}B$ process. The asymmetry of sum of the reactions forming the maximum at $E_{ex} \approx 6\,MeV$ is $\Sigma \approx 0.6$, what is less than for the previous reaction, and is close to the asymmetry of the free deuteron disintegration. As was noted in the [1], such value of the asymmetry agrees with suggestion about the $2h - 1p$ character of the $3/2^-$ $(5.02\,MeV)$ and $7/2^-$ $(6.74\,MeV)$ states, which give main contribution to the maximum at $E_{ex} \approx 6\,MeV$. The dominance the two-body mechanisms of the (γ, p) reactions in this case can reduce the asymmetry value in comparison with the one-body mechanism. Since the asymmetry is determined through interference of the reaction amplitudes, some reaction mechanisms that are caused by small amplitudes and do not affect the reaction cross section can manifest themselves in this case of asymmetry.

Later it was shown [4], if to use coordinate information of the detected events from the SSDs, the energy resolution of the telescope can be improved by decreasing the kinematic broadening. As a result, more distinct the peaks of the reactions under study in the missing energy spectra and the clearer separation of them were obtained. Therefore, firstly, the experimental data were reprocessed using information on the triggered strips of the SSDs. Secondly, simultaneously, data were obtained not only on the asymmetry, but also on the cross sections of the above reactions, since the cross sections and asymmetry are determined from the same yields of the reactions. Such an opportunity was tested in the case of the deuteron disintegration reaction, $d(\vec{\gamma}, p)n$ and was described in [5].

More accurate information on the reaction $^{12}C(\vec{\gamma}, p_{01})^{11}B$ yields allowed one to make attempt to

separate contribution of the reactions $^{12}C(\vec{\gamma},p_0)^{11}B$ and $^{12}C(\vec{\gamma},p_1)^{11}B$, and to obtain cross sections and asymmetry of these processes.

2. EXPERIMENTAL SET-UP

The measurements have been performed at the MAX-lab nuclear physics facility in Lund, described in Ref. [6] in details. The experimental set up, the coherent bremsstrahlung (CB) beam characteristics, experimental registration apparatus and technique have been described in details in the previous publications [1, 3, 4, 7], thus only brief survey and some new details of the data processing are given here.

The electron beam with energy $E_0 = 192.7\,MeV$ was extracted from the MAX-I storage ring, which worked in a stretcher mode. Then the beam was delivered into experimental area, shown in [1, 3, 6, 7], and was directed onto photon radiators, a diamond crystal of $100\mu m$ thick and $50\mu m$ Al foil, fixed in a target holder of the goniometer [3]. The beam size on the radiators was no more than $2\,mm$, and the electron current was $\sim 5...10\,nA$. The duty cycle of the beam was $df \approx 50\%$ and the divergence, estimated in [3], was no more 0.041^0 ($\sim 0.71\,mrad$). A non-interacting part of the electron beam was deflected to the beam dump by the magnet, where it was absorbed by a Faraday cup.

The post-bremsstrahlung electrons were detected by a focal plane (FP) hodoscope of the main tagger system [6]. The hodoscope consists of two rows of scintillators $25\,mm$ wide and $3.2\,mm$ thick. The coincidence requirement to overlapping 50% scintillators resulted in 62 channels for detecting the post-bremsstrahlung electrons and total tagged energy range $E_\gamma = 21.9...78.8\,MeV$. The energy resolution smoothly varied from $\Delta E_\gamma \approx 0.8\,MeV$ till $\Delta E_\gamma \approx 1\,MeV$ [3, 7].

A photon collimator was placed before the shielding wall on the distance of 214 cm from the photon radiators. It consists of heavy metal main collimator of $108.5\,mm$ long, with the variable inserts with entrance openings of 12 and $5.4\,mm$ in diameter, followed by a scrubber magnet of $\sim 100\,mm$ long and a scrubber collimator of $200\,mm$ long [6]. The above holes provided the collimation angle values $\theta_c \sim 1.1\theta_\gamma$ and $\sim 0.5\theta_\gamma$, respectively, for a point-like electron beam. ($\theta_\gamma = m_e c^2/E_0$ is the characteristic angle of bremsstrahlung, E_0 and m_e are the electron energy and mass).

Two targets, a $1.1\,mm$ CH_2 and a $1\,mm$ CD_2 thickness plates, were used for measurements that allowed to measure two processes, the carbon and deuteron photo-disintegration, simultaneously. The targets were positioned on the distance $\sim 2\,m$ from the photon collimator at angle 30^0 to the photon beam direction. The numbers of carbon nuclei per cm^2 were $N_C = 0.885 \times 10^{22}\,cm^{-2}$ for the CH_2 target and $N_C = 0.771 \times 10^{22}\,cm^{-2}$ for the CD_2 target, the number of deuteron nuclei per cm^2 was $N_D = 1.541 \times 10^{22}\,cm^{-2}$.

Protons were detected by a CsI/SSD telescope [7], placed under angle $\theta_p = 90^0$ to the beam axis. It consisted of two identical single-sided silicon strip detectors and a CsI(Tl) counter, which functioned as (ΔE) and (E) detectors, respectively. The SSDs had a thickness of 0.5 mm and 64 strips, each of $1\,mm$ width, which were paralleled in groups of two for the read-out, thus yielding an effective strip width of $2\,mm$. The CsI(Tl) detector was of cylinder shape of $12.5\,cm$ in diameter and $10\,cm$ long, housed in Al container. Its angular acceptance was determined by Monte Carlo simulation, using the GEANT-4 package, and was $\Delta\theta_p \pm 14^0$ (FWHM) for the given telescope geometry and the active area of the SSDs.

3. POLARIZED PHOTON BEAM

The polarized photon beam has been produced at process of a coherent bremsstrahlung of electrons in a diamond crystal of $100\,\mu m$ thick. The crystal was fixed in a target holder of a 3-axes goniometer, assembled from five commercial moving stages [3]. The crystal orientations is determined by two angles, θ and α (defined in Ref.[3]), and their values were taken in such a way that main contribution to the CB cross section gave one vector of the reciprocal lattice of the crystal, [0-22] for parallel (PARA) and [0-2-2] for perpendicular (PERP) directions of the polarization to the reaction plane. The CB beam spectral characteristics for various crystal orientations have been studied in [3]. They were well described by the ANB code [8] calculations.

Three beam runs of the measurements have been performed. In the first and the second runs (Run-1 and 2) the coherent peak energy was $E_{\gamma,d} \approx 51\,MeV$ and $48\,MeV$, respectively, the collimation angle of the photon beam was $\theta_c \approx 1.1\theta_\gamma$. In the Run-3 the crystal orientation was the same as in the Run-1, but the collimation angle was $\theta_c \approx 0.5\theta_\gamma$.

Spectral characteristics of the coherent bremsstrahlug beam and their stability were controlled by on-line measurements of the uncollimated CB spectra with the FP hodoscope. The measurements showed the difference between the counting rates of the odd and the even FP channels (as was discussed in [3]). In some cases, the difference remained after the normalization of the CB spectra to the amorphous spectrum from $50\,\mu m$ Al radiator (i.e., in the relative (D/Al) spectra). Such effect can be due to different background contributions to the counting rate of the odd and the even FP detectors in the diamond and Al spectra. The counting rates of the FP hodoscope counters were averaged over neighboring add and even channels.

As a whole, position of the CB peak and the spectra shape were stable during the measurements within the data accuracy, i.e., the goniometer provided good repeatability of the peak position at changing the polarization direction, and the electron beam parameters were stable with enough accuracy

in the course of the measurements. The typical relative non-collimated spectra for the PARA and PERP orientations are shown in Fig.1. They demonstrate enhancement $\beta \approx 1.35$ (enhancement or the, so-cold, coherent effect, is the ratio of the spectrum value in the CB maximum to the incoherent part of the spectrum) and a small ($\sim 1\,MeV$) difference between positions of the CB peak for the PARA and PERP orientations.

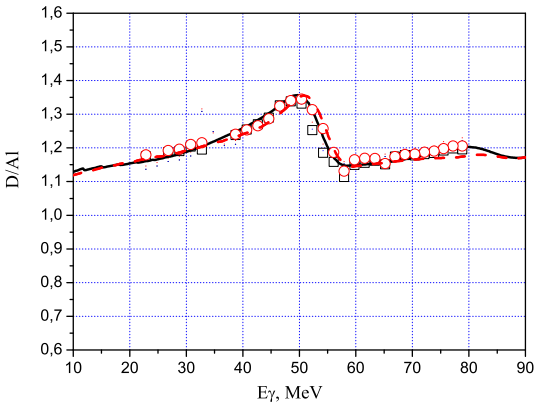

Fig.1. *Non-collimated relative D/Al spectra of the CB beam for the PARA (squares) and PERP (circles) orientations, Run-1. Curves are results of the fit for the PARA (solid) and PERP (dashed) orientations, see text for details*

The theoretical descriptions of the experimental CB spectra were performed using the ANB code [8]. At the calculations, the angles of the crystal orientation (θ and α), and some constant background contribution to the incoherent part of the spectra were the fitting parameters, values of which were determined by fitting the theoretical spectrum to the experimental one by a FUMILI code. The fit was performed, firstly, because of the indication on the background contribution to the FP counting rate, as noted the above, and secondly, because of the need to refining the orientation angles due to a possible change in the "zero" angles [3] in the process of changing the polarization direction. The fit allowed one to describe more accurate the experimental spectra in all tagging energy interval, Fig.1. The values of the orientation angles, obtained from the fit, coincided with the experimental values for the PERP orientations for both peak energies, but for the PARA orientations there was a $\sim$ 10% difference between these values. The background contribution to the FP detectors counting rate in the range of the CB peak was $\sim$ 5...15% for all orientations. Calculated polarization of the non-collimated beam in the CB maximum was $P_\gamma \approx 0.17$.

The spectra and polarization of the beam incident on the nuclear targets were calculated by the ANB code, using the orientation angle values, obtained by the fit, and taking into account the photon beam collimation and other experimental parameters that were used for the non-collimated spectra description.

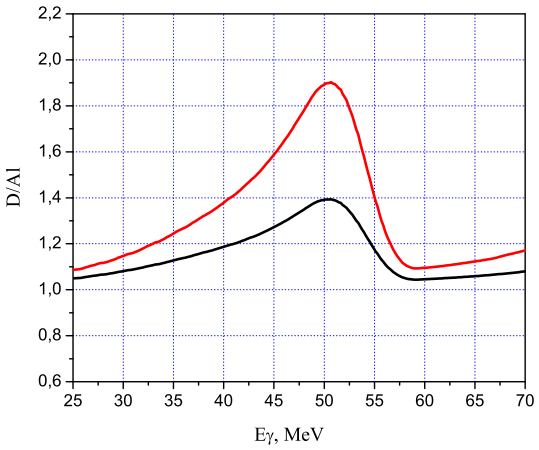

Fig.2. *Calculated spectra of the CB beam averaged over PARA and PERP orientations. Collimation angles $\theta_c \approx 1.1\theta_\gamma$ (Run-1, down) and $\theta_c \approx 0.5\theta_\gamma$ (Run-3, upper)*

The calculated spectra and polarization of the beam for the PARA and PERP orientations were close in shape, so they were average. The results are shown in Fig.2, and some results for the collimation angle $\theta_c \approx 1.1\theta_\gamma$ have been presented in Ref.[5]. The calculations have shown that even weak collimation, $\theta_c \approx 1.1\theta_\gamma$, increases the coherent effect and the polarization in the CB maxima to $\beta \approx 1.4$ and $P_\gamma \approx 0.25$. The stronger collimation $\theta_c \approx 0.5\theta_\gamma$, being in the Run-3, increases the enhancement and the polarization to $\beta \approx 1.9$ and $P_\gamma \approx 0.42$.

4. DATA ANALYSIS

The data analysis was divided into three parts. The first consists of selection protons from other particles, calculation their energy and energy of the photon, producing the reaction. The second part includes description of the background spectra generation, their subtraction, and extraction of the reaction yields. The third consists of determination experimental factors, such as solid angle, tagging efficiency, stolen corrections and calculation of the cross sections and the asymmetry. The first part and some details of the other parts of the analysis have been described in the previous works [1, 5, 7], thus only brief survey and new details of the data processing are given here.

Protons were identified by standard $\Delta E - E$ method, based on relationship between energy losses ΔE and full energy E of the particles with different masses. The two-dimensional plot pairs of ADC signals from the SSD and the CsI detectors of the telescope (see Fig.3 in Ref. [7]) allowed to separate protons from other particles into clear band and to remove the background particles by special soft cut.

Energy losses of the protons on their way from the target to the CsI detector were calculated by Monte Carlo simulation. Using the losses, the energy deposited by protons in the detectors was obtained, and a correlation between the deposited energy and the amplitude of the CsI detector signal

was determined. It demonstrated linear dependence between the energy of incoming proton and the CsI signal within energy interval of $T_p = 10...50\,MeV$. The proton detection threshold by the telescope was $T_{th} \approx 18\,MeV$ that corresponded to the photon energy of $E_{\gamma,th} \approx 40\,MeV$ for the $d(\gamma,p)n$ reaction, and $E_{\gamma,th} \approx 36\,MeV$ for the $^{12}C(\vec{\gamma},p_0)^{11}B$ reaction when the ^{11}B nucleus was in the ground state.

The coincidences between signals of the SSDs and the CsI detector, corresponding to the proton band, (shown in Fig.3, Ref. [7]) generated trigger signals, which started the time measurements for all FP detectors. After correction of the trigger signals for time walk, a strong prompt peak of the time coincidence of the FP detectors and CsI/SSD telescope signals (FPtdc) was obtained on top of random background in the individual tagger TDCs, see [1, 7] for details. The time resolution of the FPtdc coincidence was $\sim 2...3\,ns$. In order to enable summing the FPtdc spectra, the prompt peaks for all FP channels were shifted to the channel number 750 of the FPtdc. From the Gauss fit the position μ and the standard deviation σ of the peaks were determined. The range $\mu \pm 3\sigma$ defined the prompt region. It includes events both from reactions of the deuteron and the carbon disintegration, and the random background. The region to the right of the prompt peak includes only random events, which were taken for the background spectra generation, see [1, 7].

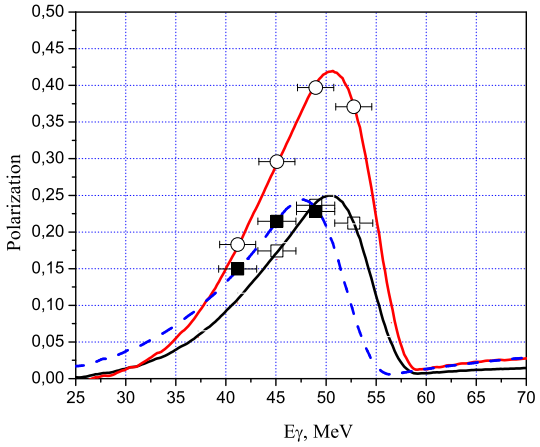

Fig.3. *Calculated polarization of the CB beam, averaged over PARA and PERP orientations, for the collimation angle $\theta_c \approx 1.1\theta_\gamma$ (Run-1 (solid), Run-2 (dashed), and the $\theta_c \approx 0.5\theta_\gamma$ (Run-3 (upper line)). Points are the polarization averaged over energy bins, which were used for the asymmetry calculation, see text*

Each focal plane channel defines the disintegration reaction uncorrelated with the others. In order to increase statistics, summation of excitation energy spectra (see below) for four physically adjacent FP channels was made. As a result, for Run-1 and 2 the excitation energy spectra have been obtained for twelve energy bins for measurements on both targets. The central energies of the bins were: $E_\gamma = 37.2$, 41.2, 45.1, 49.0, 52.8, 56.5, 60.2, 63.8, 67.3, 70.8, 74.3, and $77.7\,MeV$. The bin's energy width varied from $\Delta E_\gamma \approx 4$ for the first bin at energy $E_\gamma = 37.2\,MeV$, to $3.4\,MeV$ for the end bins at the energy $E_\gamma = 77.7\,MeV$. For the Run-3, the spectra were obtained for measurements on the CD_2 target only and for the energy bins around the CB peak, $E_\gamma = 37.2$, 41.2, 45.1, 49.0, 52.8, 56.5, $60.2\,MeV$, because of small statistic at higher energies.

The polarization was averaged over width of the bins in the range of the CB maximum, and for the asymmetry calculation only those bins were used, for which the polarization value was $P_\gamma > 0.15$, as is shown in Fig.3.

4.1. THE REACTIONS SELECTION. SPECTRA OF EXCITATION ENERGY

For separation the $^{12}C(\vec{\gamma},p)^{11}B$ reactions, corresponding to low lying ^{11}B exited states, spectra of excitation energy (ExE) were produced, by taking events from the prompt region of the FPtdc spectra. The excitation energy of the reaction is defined as,

$$E_{ex} = E_\gamma - T_p - T_r + Q_{gs}, \qquad (2)$$

where E_γ is the energy of the tagged photon, T_p is the kinetic energy of the detected proton, measured by the CsI detector and corrected to energy losses on the way from the origin point to the detector, T_r is the energy of the recoil nucleus ^{11}B, calculated by the two-body kinematics, using of the photon energy and the proton emission angle values, Q_{gs} is the Q-value of the reaction, leading to the ^{11}B ground state. The excitation energy spectra were constructed for all energy bins for both targets. The spectra have typical shape, shown in Fig.4, identical for all bins.

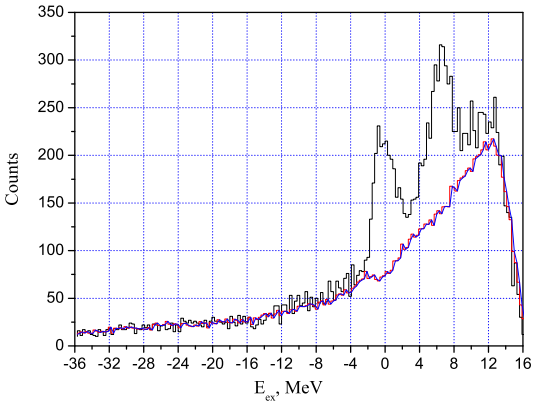

Fig.4. *Excitation energy spectra of $^{12}C(\vec{\gamma},p)^{11}B$ reaction measured on CD_2 target in Run-1 for the PARA orientation. Photon energies are $E_\gamma = 49.0 \pm 1.9\,MeV$. The lower line is the random background spectrum, see text for details*

They have maxima resulted from reactions of the carbon (and deuteron disintegration, when measurements perform on the CD_2 target), which are on top of the random background from the prompt region

of the FPtdc. Coordinate information from the SSDs triggered strips were used in order to decrease the kinematical broadening of the peaks (see Ref. [4] for details).

For the background subtraction, the corresponding random background spectra were generated from events of the random range of the FPtdc spectra.

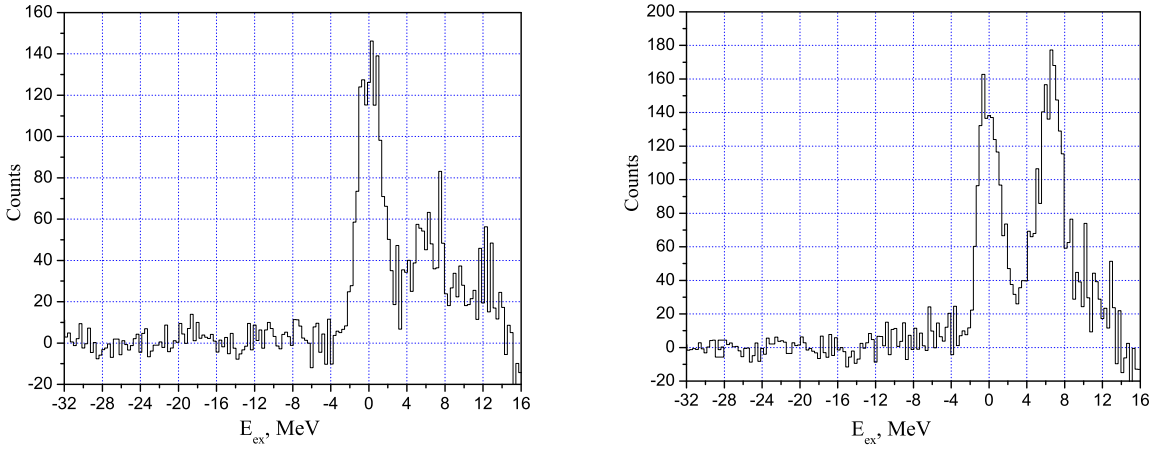

Fig.5. *Excitation energy spectra of* $^{12}C(\vec{\gamma},p)^{11}B$ *reaction for the* CH_2 *(left) and* CD_2 *(right) targets.* $E_\gamma = 49.0 \pm 1.9\,MeV$. *Run-1, PARA*

They were normalized to the prompt background of the ExE spectra in the range to the left from the first peak of the carbon disintegration, Fig.4. Details of the normalization procedure have been discussed in [5].

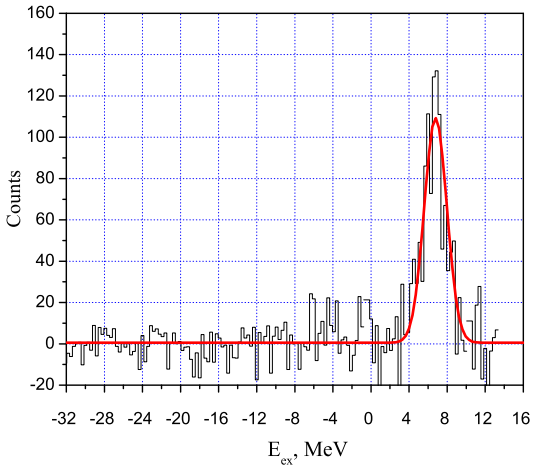

Fig.6. *Excitation energy spectra of* $d(\vec{\gamma},p)n$ *reaction for* $E_\gamma = 49.0 \pm 1.9\,MeV$. *Run-1, PARA*

After the background subtraction, the excitation energy spectra have typical shape shown in Fig.5. Firstly, they have prominent peak at $E_{ex} \approx 0$ which resulted from unresolved the $3/2^-$(ground state) and the first exited state $1/2^-$ $(2.12\,MeV)$ of the ^{11}B, and secondly, the peak centered around $E_{ex} \approx 6\,MeV$ (in the spectrum for the CH_2 target), resulted from excitation of the $1/2^-$ $(4.45\,MeV)$, $3/2^-$ $(5.02\,MeV)$, $7/2^-$ $(6.74\,MeV)$, $1/2^+$ $(6.79\,MeV)$ and $5/2^+$ $(7.29\,MeV)$ states. To the left side from the carbon disintegration peaks there is the random background range. The background spectrum in this range oscillates near zero value that confirms correctness of the normalization and the background subtraction.

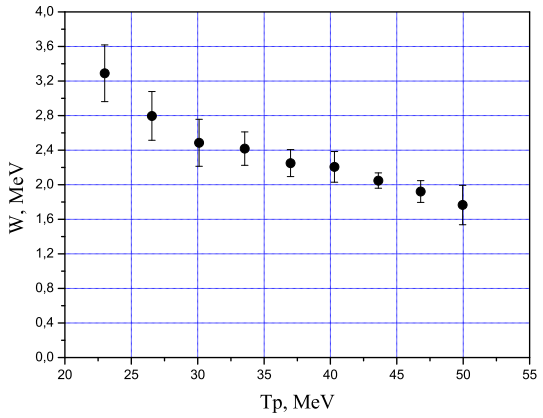

Fig.7. *Energy resolution (FWHM) as a function of the proton energy*

There is also a peak of the deuteron disintegration in the spectrum obtained from the CD_2 target, position of which for this photon energies is at $E_{ex} \approx 7\,MeV$ and coincides with position of the second peak of the carbon disintegration. The deuteron peak is displaced to higher energies with the photon energy increasing, while the positions of the carbon disintegration peaks do not change, and for energies $E_\gamma \geq 56.5\,MeV$ the deuteron and second carbon peaks are well separated. The subtraction of the CH_2 excitation energy spectra from the corresponding CD_2 ones gives the ExE spectra for the $d(\gamma,p)n$ reaction. As example, such spectrum is shown in Fig.6. It demonstrates clear the deuteron peaks and accurate the background subtraction in the entire energy interval.

It should be noted that after decreasing of the

kinematical broadening influence, the energy resolution is mainly resulted from fluctuations of the proton ionization losses on their path from the point of origin to the CsI detector, which decrease with the proton energy increasing, so the resolution should be improved. It was estimated from dependence of the first peak width (FWHM) of the ExE spectra, obtained from the Gauss fit, viz. a function of the proton energy. The results are presented in Fig.7 and demonstrate that the resolution is changed from $\sim 3.3\,MeV$ to $\sim 2\,MeV$ for the proton energies corresponding to the photon tagging energy interval $E_\gamma \approx 40...78\,MeV$.

4.2. THE REACTION YIELDS

Yields of the reactions, both the deuteron and the carbon disintegration, were obtained from the corresponding excitation energy spectra, Figs.5 and 6. The $d(\vec{\gamma},p)n$ reaction yield was calculated by two ways described in detail in [5, 7]. Firstly, by fit of the peak by Gaussian and calculation the reaction yield according to the formula,

$$Y_p = \frac{A}{w}, \tag{3}$$

where $A = \sqrt{2\pi}\sigma Y_m$ is the square of the Gaussian, Y_m is the Gaussian maximum height, σ is the standard deviation of the peak, and $w = 0.3\,MeV$ is the width of the step in the excitation energy spectrum construction. Secondly, the reaction yields were obtained by summation the events in the peak region, $\mu \pm 3\sigma$, where μ is the peak position.

Because of threshold of the $d(\vec{\gamma},p)n$ reaction detection, $E_{\gamma,th} \approx 40\,MeV$, the yields were obtained for 10 energy bins for the Run 1 and 2, starting from the bin $E_\gamma = 45.1 \pm 2\,MeV$. The yields of the $d(\vec{\gamma},p)n$ reaction, obtained by these two methods, were coincided with a good accuracy. The statistical accuracy of the yields varied from $\sim 10\%$ at $E_\gamma = 45.1 \pm 2\,MeV$ to $\sim 20\%$ for $E_\gamma = 77.6 \pm 1.7\,MeV$.

4.2.1. YIELD OF THE CARBON DISINTEGRATION REACTIONS

As was noted the above, only two maxima of the carbon disintegration reactions were observed in the ExE spectra. The first maximum results from the ground and the first $1/2^-$ $(2.12\,MeV)$ exited states of the ^{11}B, but an according to the reaction cross section data [9], contribution from the $2.12\,MeV$ state is $\sim 20\%$ at the photon energies $E_\gamma \approx 44...52\,MeV$. As to the second peak, which is centered around $E_{ex} \approx 6\,MeV$, it is formally formed by the five states, but actually resulted from two states, $3/2^-$ $(5.02\,MeV)$ and the $7/2^-$ $(6.74\,MeV)$, which give main contribution [10, 11]. Thus, four Gaussians were involved for description of the ExE spectra,

$$y = y_0 + \sum_i A_i e^{-\frac{(x-x_i)^2}{2\sigma_i^2}}, \tag{4}$$

where y_0 is the constant, A_i is the height, x_i is the positions of the maximum, σ_i is the standard deviation related to the peak FWHM by the formula $W_i = 2.35\sigma_i$, and $i = 0,\ 1,\ 2,\ 3$. Most of these parameters were fixed. Firstly, the positions of the Gaussian maxima, were fixed at the excitation energy values: $x_i = 0,\ 2.12,\ 5.02$ and $6.74\,MeV$, respectively. Secondly, the widths of the Gaussians (W_i) were fixed at the values, corresponding to the energy of detected protons, emitted from the reactions with the above excited states of the ^{11}B, according to the dependence, shown in Fig.7. The other parameters were the fitting ones. On the whole, the fit (4) satisfactory describes the ExE spectra in whole energy range for both targets. Some typical examples of the fits are shown in Fig.8.

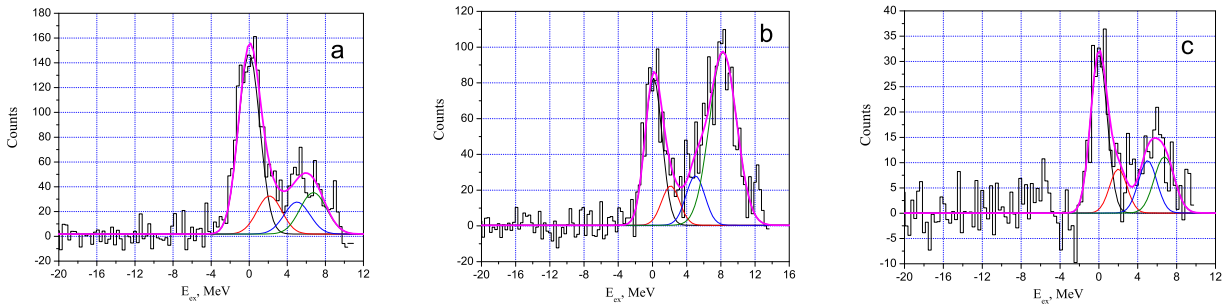

Fig.8. *Excitation energy spectrum of $^{12}C(\vec{\gamma},p)^{11}B$ reaction: a) for $E_\gamma = 45.1 \pm 2\,MeV$. CH_2 target, PARA, Run-1; b) for $E_\gamma = 52.8 \pm 1.9\,MeV$. CD_2 target, PARA, Run-1; c) for $E_\gamma = 60.2 \pm 1.8\,MeV$, CH_2 target, PERP, Run-1. The solid lines are results of fitting*

The yields of the $^{12}C(\vec{\gamma},p_{01})^{11}B$ and the $^{12}C(\vec{\gamma},p_{2-6})^{11}B$ reactions were obtained from the CH_2 target ExE spectra for the energy bins $E_\gamma \geq 41.2$ and $45.1\,MeV$, respectively. In the case of measurements on the CD_2 target, the yields of the $^{12}C(\vec{\gamma},p_{01})^{11}B$ and the $^{12}C(\vec{\gamma},p_{2-6})^{11}B$ reactions were obtained for the energy bins $E_\gamma \geq 45.1$ and $56.5\,MeV$, respectively, because of the deuteron dis-

integration contribution. At that, although for energy bins $E_\gamma = 45.1$, 49.0 and 52.8 MeV the deuteron maximum is in the region of the second peak of the ExE spectra, but it gives else some contribution to the first maximum. In order to subtract this contribution correctly, the positions and the widths of the third and the fourth Gaussians were not fixed, but also taken as fitting parameters. For the energies $E_\gamma \geq 56.5\,MeV$, the deuteron peak is shifted above the second peak position, and yields of the $^{12}C(\vec{\gamma}, p_{2-6})^{11}B$ reaction are also possible to get .

For Run-3 the yields of the $^{12}C(\vec{\gamma}, p_{01})^{11}B$ reaction were only obtained from the CD_2 target ExE spectra for energies up to $E_\gamma = 60.2\,MeV$, due to poor statistics for higher energies. The energy resolution at higher energies becomes a little better, thus first exited state $E_{ex} = 2.12\,MeV$ display itself noticeably by distorting the shape of the first maximum, as shown in Fig.8, that allow to separate contribution from ground and the first excited states more accurately.

The yields corresponding to each Gaussian, obtained from the fit, were calculated by the formula (3), and then the yields of the $^{12}C(\vec{\gamma}, p_{01})^{11}B$ and the $^{12}C(\vec{\gamma}, p_{2-6})^{11}B$ reactions were obtained by summation the yields of the first and the second pairs of the Gaussians, respectively. For control, direct summation of the events under the first and the second peaks was performed, as well, for the energy bins, for which it was possible. Because position of these maxima were constant, the summation limits were determined from the Gauss fit results and were $E_{ex} = -4...3.8\,MeV$ and $E_{ex} = 4.1...9\,MeV$ for the first and the second peaks, respectively. The yields of the $^{12}C(\vec{\gamma}, p_{01})^{11}B$ and the $^{12}C(\vec{\gamma}, p_{2-6})^{11}B$ reactions obtained by the fit and summation of the spectra events well agreed, as well as, in the case of the $d(\vec{\gamma}, p)n$ reaction [5].

As a whole, the yields of the $^{12}C(\vec{\gamma}, p_{01})^{11}B$ reaction were obtained in the total interval $E_\gamma = 41.2...74.2\,MeV$ with good statistics in the range of the CB peak ($E_\gamma = 41.2...60.2\,MeV$), where each energy was measured six times, and four times for the higher energies. The yields of the $^{12}C(\vec{\gamma}, p_{2-6})^{11}B$ reaction were obtained in the interval $E_\gamma = 45.1...74.2\,MeV$ and each energy was measured four times.

4.3. CROSS SECTIONS AND CROSS SECTION ASYMMETRY CALCULATION

Differential cross sections were obtained by the formula, which was used earlier in Ref.[5] for calculation the cross sections in the case of the polarized photon beam,

$$\frac{d\sigma}{d\Omega} = \frac{1}{2N_A\Delta\Omega}\left(\frac{Y_{p,\parallel}}{N_{\gamma,\parallel}\varepsilon_{st,\parallel}} + \frac{Y_{p,\perp}}{N_{\gamma,\perp}\varepsilon_{st,\perp}}\right), \qquad (5)$$

where $Y_{p,\parallel(\perp)}$, $\varepsilon_{st,\parallel(\perp)}$, $N_{\gamma,\parallel(\perp)}$, are the reaction yield, the stolen correction, the photon flux incident on the target, respectively, corresponding to the measurements at the PARA (PERP) orientations of the photon beam polarization. N_A is the number of the target nuclei per area, presented the above. $\Delta\Omega$ is the effective solid angle of the CsI/SSD telescope. It was determined in the previous Ref. [7] and was $\Delta\Omega = 249.00 \pm 2.25\,msr$.

The photon flux was determined by the relation,

$$N_{\gamma,\parallel(\perp)} = \varepsilon_{tag} \cdot N'_{e,\parallel(\perp)}, \qquad (6)$$

where $N'_{e,\parallel(\perp)}$ is the number of the post-bremsstrahlung electrons, detected by the FP detectors at the PARA (PERP) orientations, and ε_{tag} is the CB beam tagging efficiency, which should be identical for both orientations. In the case of the CB beam, the tagging efficiency depends on the beam collimation and the coherent peak position. For the conditions that were in the Run-1 and 2 ($E_{\gamma,d} \approx 51$ and $48\,MeV$, the collimator opening of $12\,mm$ in diameter), the tagging efficiencies were obtained in the previous work [5]. For the conditions that were in the Run-3 ($E_{\gamma,d} \approx 51\,MeV$, the collimator opening of $5.4\,mm$), it was calculated in the present work by the same way. The tagging efficiencies for the PARA and PERP orientations were almost the same in each run, so they were averaged. In general, the tagging efficiencies for the collimation angles $\theta_c \approx 1.1\theta_\gamma$ and $\theta_c \approx 0.5\theta_\gamma$ were close in the shape and had a maximal value at the CB maximum energy, $\varepsilon_{tag} = 0.36$ and 0.12, respectively. After the peak energy, they decreased to $\varepsilon_{tag} = 0.32$ and 0.08, and then increased slightly with the photon energy increasing.

The stolen correction to the reaction yields resulted from the fact that the uncorrelated electron can be registered in the region to the left of the prompt peak, thus a focal plane TDC can be stopped by a random electron, arriving earlier than a correlated one. The value of the stolen correction depends on the counting rate in the focal-plane detectors, the beam duty factor, and the position of the lower limit of the prompt region in the FPtdc spectrum (see Ref. [5] for details), thus its value depend on the photon energy. The position of the lower limit of the prompt peak was constant for all measurements, the duty factor and the counting rates of the focal plane detectors were also close for all runs, so the stolen corrections were practically identical for all runs. Its value changed from $\sim 30\%$ at $E_\gamma = 45\,MeV$ to $\sim 14\%$ at $E_\gamma = 78\,MeV$.

The cross section asymmetry was obtained using the same proton yields, $Y_{p,\parallel(\perp)}$, which were used for the cross sections calculation. It is given by

$$\Sigma = \frac{1}{P_\gamma}\frac{\frac{Y_{p,\parallel}}{N_{\gamma,\parallel}\varepsilon_{st,\parallel}} - \frac{Y_{p,\perp}}{N_{\gamma,\perp}\varepsilon_{st,\perp}}}{\frac{Y_{p,\parallel}}{N_{\gamma,\parallel}\varepsilon_{st,\parallel}} + \frac{Y_{p,\perp}}{N_{\gamma,\perp}\varepsilon_{st,\perp}}}, \qquad (7)$$

where P_γ is polarization of the photon beam. The asymmetry was calculated for the energy bins in the range of the CB maximum, for which the polarization degree was $P_\gamma \geq 0.15$. This condition restricted the number of the asymmetry values to be obtained:

four points for the $^{12}C(\vec{\gamma}, p_{01})^{11}B$ reaction with energies, E_γ = 41.2, 45.1, 49.0, 52.8 MeV, and three points for the $^{12}C(\vec{\gamma}, p_{2-6})^{11}B$ reaction with energies E_γ = 45.1, 49.0, 52.8 MeV.

The systematic uncertainty was estimated to be $\sim$ 10%, and arises from error of the random background spectra normalization at the background subtraction ($\sim$ 7%), and accuracy of the polarization determination ($\sim$ 5%).

5. DISCUSSION OF THE RESULTS

Measurement of the reaction of deuteron disintegration was performed to verify data processing and control of the experimental parameters, such as solid angle, target efficiency and beam polarization.

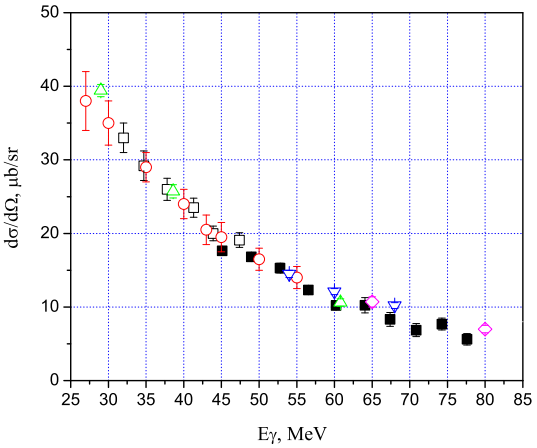

Fig.9. *Cross section of the $d(\gamma, p)n$ reaction average over Run-1 and Run-2 measurements (squares). Data [13] – empty squares; [14] – triangles down; [15] – triangles up; [16] – empty circles; [17] – rhombus*

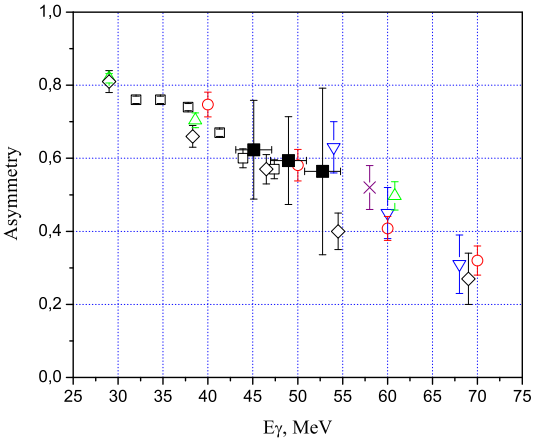

Fig.10. *Asymmetry of the $d(\vec{\gamma}, p)n$ reaction average over Run-1 and Run-2 measurements. Data [13] (empty squares), [14] (triangles down), [15] (triangles), [22] (rhombus). [23] (circles), [24] (crosses)*

In the previous work [5], various variants of data processing were studied in detail, and experimental parameters were determined. The obtained the $d(\gamma, p)n$ reaction cross sections and the asymmetry were in good agreement with the existing data [5].

In the present work, the cross sections and asymmetry of the reactions of the carbon and deuteron disintegration, $d(\gamma, p)n$, $^{12}C(\vec{\gamma}, p)^{11}B$ and $^{12}C(\vec{\gamma}, p_{01})^{11}B$, were obtained simultaneously from the same excitation energy spectra. The cross section and asymmetry obtained from measurements in all runs and for both targets were close, thus they were averaged. The results for the $d(\gamma, p)n$ reaction are presented In Figs.9 and 10. Both the cross sections and the asymmetry well agree with the literature data within the data accuracy.

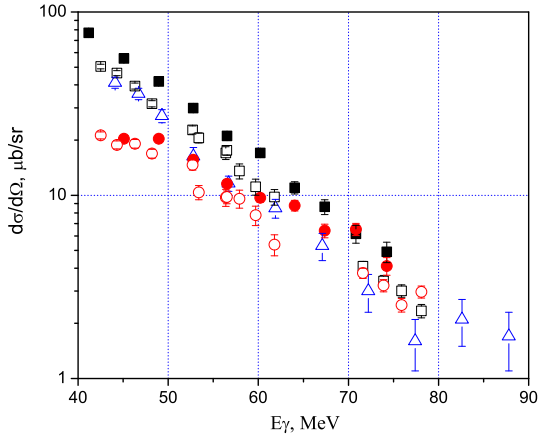

Fig.11. *Cross sections of the carbon disintegration. $^{12}C(\gamma, p_{01})^{11}B$ reaction: this experiment for proton emission angle θ_p = 85^0 (full squares), data [9] (empty squares) and [18] (empty triangles) for θ_p = 90^0. $^{12}C(\gamma, p_{2-6})^{11}B$ reaction: this experiment for θ_p = 85^0 (full circles), data [9] on the $^{12}C(\vec{\gamma}, p_{2-6})^{11}B$ (empty circles)*

The measured cross sections of the $^{12}C(\gamma, p_{01})^{11}B$ and the $^{12}C(\gamma, p_{2-6})^{11}B$ reactions, averaged over all measurements cover the energy intervals E_γ = 41...78 MeV and E_γ = 45...78 MeV, respectively, and are presented in Fig.11. They demonstrate typical energy dependencies which are different for these reactions. The $^{12}C(\gamma, p_{2-6})^{11}B$ cross sections slower decrease with the photon energy increasing, so that at $E_\gamma \sim$ 70...80 MeV the cross sections for both reactions become close. Such behavior points out that these reactions have different mechanisms. The obtained cross sections well agree with literature data if to take into account that effective angle of the measurement was $\theta_p \approx 85^0$, due to large angular acceptance of the telescope and strong angular dependence of the reactions. It can be seen in Fig.12 where the angular distributions of the cross sections are presented.

The asymmetry or the $^{12}C(\vec{\gamma}, p_{01})^{11}B$ and the $^{12}C(\vec{\gamma}, p_{2-6})^{11}B$ reactions is shown in Fig.13. The measurements cover energy interval $\sim$ 40...55 MeV for the $(\vec{\gamma}, p_{01})$ and 43...52 MeV for the $(\vec{\gamma}, p_{2-6})$ reactions. One can see that new data processing results in the same values of the asymmetry of the

$^{12}C(\vec{\gamma}, p_{01})^{11}B$ reaction as well as in the previous work [1], except for one point at $E_\gamma = 41\,MeV$.

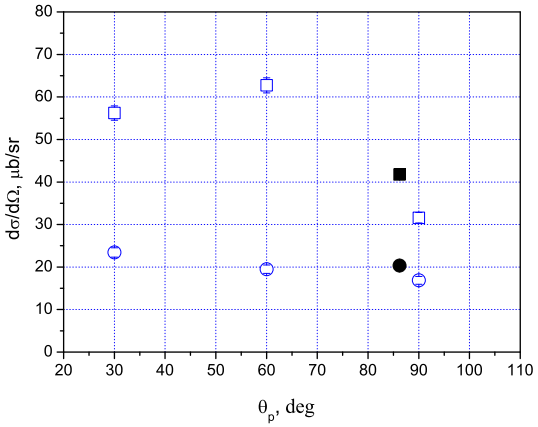

Fig.12. *Angular dependence of the $^{12}C(\gamma, p_{01})^{11}B$ (squares) and $^{12}C(\gamma, p_{2-6})^{11}B$ (circles) reaction cross sections for $E_\gamma = 48.2\,MeV$. Empty points are data [9]*

As to the asymmetry of the $^{12}C(\vec{\gamma}, p_{2-6})^{11}B$ reaction, new data are somewhat higher, but as a whole, they agree with the previous results [1] within the data accuracy.

As was noted in the previous work [1], the cross section asymmetry of sum of the reactions forming the first maximum and the second maxima is $\Sigma \approx 0.8$ and $\Sigma \approx 0.6$.

From the experimental data on the cross section [9] and the relative contributions of the states forming the second peak [10], one can assume that the asymmetry is resulted from the ground state, which have 1h character, in the first case, and from the $7/2^-$ $(6.74\,MeV)$ and the $3/2^-$ $(5.02\,MeV)$ states, in the second case, which have 2h-1p character, and can be realized due to the two-body mechanisms of the reaction.

The RPA calculations prediction agree well with the experimental data for the $^{12}C(\vec{\gamma}, p_{01})^{11}B$ reaction, but have significant discrepancy with the data for $^{12}C(\vec{\gamma}, p_{2-6})^{11}B$ reaction, which agree well with the QD model predictions in the energy range under study. The quasi-deuteron model predicts another energy dependence of the asymmetry than RPA, close to the free deuteron photodisintegration, but $\sim 15...20\%$ higher than the experimental data for free deuteron disintegration [15, 16].

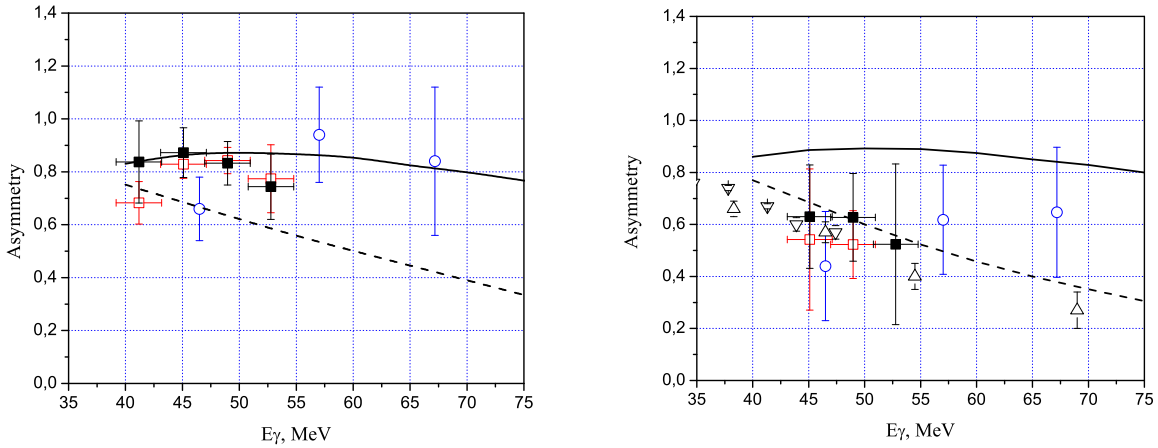

Fig.13. *Left: Asymmetry of the $^{12}C(\vec{\gamma}, p_{01})^{11}B$ reactions averaged over three runs and CH_2 and CD_2 targets. Circles are the data J.Yokokawa et al. [25] for the sum of $E_{ex} < 5\,MeV$. Right: Asymmetry of the $^{12}C(\vec{\gamma}, p_{2-6})^{11}B$ reactions averaged over three runs CH_2 targets. Circles are the J.Yokokawa et al., [25] for the sum of $E_{ex} > 5\,MeV$, triangles (up) and (down) are the data [22] and [13] on the $d(\vec{\gamma}, p)n$ reactions. Curves are prediction by the RPA theory (solid lines) and quasi-deuteron model (dashed lines) [25]*

As a whole, such behavior of the asymmetry agree with suggestion about the $2h-1p$ character of the $E_{ex} = 5.02$ and $6.74\,MeV$ states and dominating the two-body mechanisms of the (γ, p) reactions in this case, which can decrease the asymmetry value in comparison with the one-body mechanism. The (γ, p) reactions leading to $2h-1p$ states is dominated by pionic effects.

The measured cross sections of the $^{12}C(\gamma, p_{01})^{11}B$ reaction well agree with the existing literature data. This fact gives a confidence that the Gaussians correctly determine the contribution of the ground and the first excited states to the first peak, and one can to get cross sections and the asymmetry of the $^{12}C(\vec{\gamma}, p_0)^{11}B$ and the $^{12}C(\vec{\gamma}, p_1)^{11}B$ reactions. The corresponding results are shown in Figs.14-16, and presented in the Tables 1 and 2. The obtained cross sections of the $^{12}C(\gamma, p_0)^{11}B$ and the $^{12}C(\gamma, p_1)^{11}B$ reactions well agree with the data [9] and well reproduce the energy dependences of the reactions, which are identical for both these processes. The cross section asymmetry of the $^{12}C(\vec{\gamma}, p_0)^{11}B$ reaction is practically identical to the $^{12}C(\vec{\gamma}, p_{01})^{11}B$ reaction asymmetry. For the reaction $^{12}C(\vec{\gamma}, p_1)^{11}B$ the asymmetry

is determined with less accuracy, but its value is less than for the $^{12}C(\vec{\gamma},p_0)^{11}B$ reaction.

In Fig.16 the angular dependencies of the reactions $^{12}C(\gamma,p_0)^{11}B$ and $^{12}C(\gamma,p_1)^{11}B$ from [21] are presented.They are well described by the coherent sum of one hole (1h) and the $2h-1p$ mechanisms.

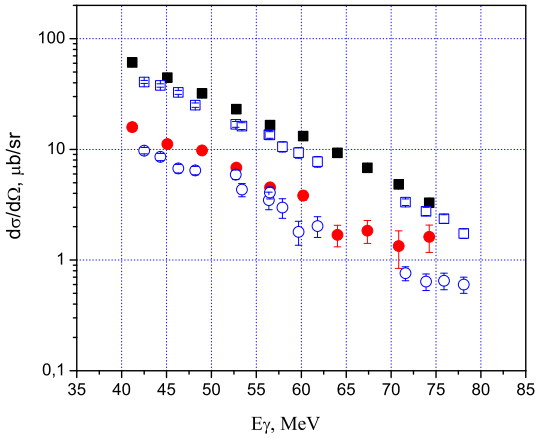

Fig.14. *Cross sections $^{12}C(\gamma,p_0)^{11}B$ (squares) and $^{12}C(\gamma,p_1)^{11}B$ (circles) reactions, averaged over all measurements. Empty points are data [9]*

In the case $^{12}C(\gamma,p_0)^{11}B$ reaction, the one hole mechanism gives main contribution and practically describes the experimental data, because the $2h-1p$ mechanisms contribution is small. But the one hole mechanism produces large asymmetry. The experiment has shown that asymmetry of the $^{12}C(\gamma,p_0)^{11}B$ process is rather high, $\Sigma \approx 0.85$.

In the case of the $^{12}C(\gamma,p_1)^{11}B$ reaction, the theory somewhat worse describes the $^{12}C(\gamma,p_1)^{11}B$ cross sections. But the relative contribution of the $2h-1p$ mechanism to the cross section is more than in the case of the $^{12}C(\gamma,p_0)^{11}B$ reaction.

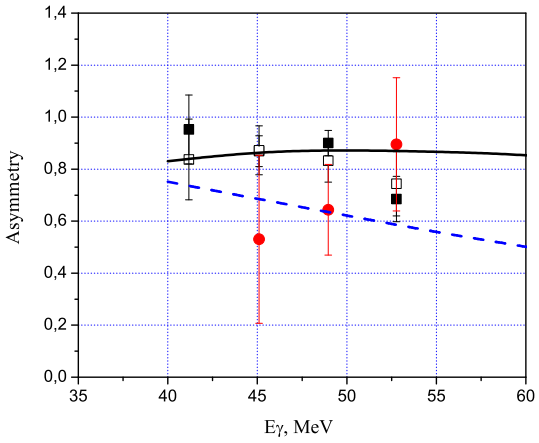

Fig.15. *Asymmetry of the reactions $^{12}C(\vec{\gamma},p_0)^{11}B$ (empty squares), the $^{12}C(\vec{\gamma},p_1)^{11}B$ (triangles) and the $^{12}C(\vec{\gamma},p_{01})^{11}B$ (full squares) averaged over three runs and CH_2 and CD_2 targets. Circles are the data J. Yokokawa et al. [25] for the sum of $E_{ex} > 5\,MeV$, triangles (up) and (down) are the data [22] and [13] on the $d(\vec{\gamma},p)n$ reactions. Curves are prediction by the RPA theory (solid lines) and quasi-deuteron model (dashed lines) from [25]*

Because the two-body mechanism gives less asymmetry, the asymmetry of the $^{12}C(\gamma,p_1)^{11}B$ reaction should be less that is confirmed by the experimental results, as can be seen in Fig.15.

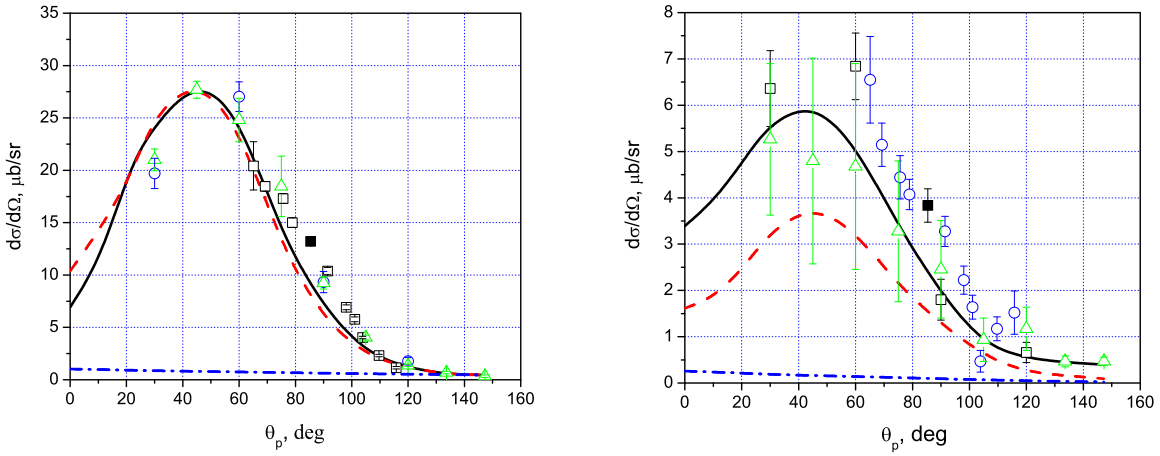

Fig.16. *Angular dependence of the cross sections $^{12}C(\gamma,p_0)^{11}B$ (left) and $^{12}C(\gamma,p_1)^{11}B$ (right) for $E_\gamma = 60\,MeV$. Experimental data: full squares are this experiment, [9]- circles, [19] – triangles, [20] - empty squares. The curves from [21] – the dotted line gives the 2h-1p contribution, the dashed line is the hole contribution, and the solid line is their coherent sum*

6. SUMMARY

The cross section and cross section asymmetry of the $^{12}C(\vec{\gamma},p_0)^{11}B$ and $^{12}C(\vec{\gamma},p_1)^{11}B$ reactions was measured using the linearly polarized photon beam of the MAX-lab facility in the energy ranges $E_\gamma \sim 40...78\,MeV$ and $\sim 40...55\,MeV$, respectively. The

cross sections of the both reactions well agree with the literature data.

The beam asymmetry of the $^{12}C(\vec{\gamma},p_0)^{11}B$ reaction when the final nucleus is in the $3/2^-$ (ground state) is rather high, $\Sigma \approx 0.85$ and agree well with the RPA model calculations. It have significant discrepancy with the quasideuteron model predictions and mainly determined by the one hole mechanism.

The asymmetry of the $^{12}C(\vec{\gamma},p_1)^{11}B$ reactions is less, $\Sigma \sim 0.6...0.7$, due to more relative contribution of the $2h-1p$ mechanism to the dominating one hole.

References

1. D. Burdeinyi, J. Brudvik, K. Fissum, V. Ganenko et al. // *Nuclear Physics.* 2017, A957, p.321-331.
2. V. Ganenko, K. Fissum, K. Hansen, et al. // *Problems of Atomic Science and Technology. Series "Nuclear Physics Investigations".* 2009, N3(51), p.95-102.
3. V. Ganenko, J. Brudvik, D. Burdeinyi et al. // *Nucl. Instr. and Meth.* 2014, v.A763 p.137-149.
4. J. Brudvik, D. Burdeinyi, V. Ganenko et al. // *Problems of Atomic Science and Technology.* 2016, N3(103), p.111-116.
5. J. Brudvik, D. Burdeinyi, V. Ganenko et al. // *Problems of Atomic Science and Technology.* 2018, N3(115), p.132-139.
6. J.-O. Adler et al. // *Nuclear Instruments and Methods in Physics Research.* 2013, v.A715, p.1-10.
7. J. Brudvik, D. Burdeinyi, V. Ganenko, K. Hansen et al. // *Problems of Atomic Science and Technology.* 2015, N3(97), p.49-64.
8. F.A. Natter et al. // *NIM.* 2003, v.B211, p.465.
9. H. Ruijter et al. // *Phys. Rev.* 1996, v.C54, p.3076.
10. A. Kuzin et al. // *Phys. Rev.* 1998, v.C58, p.2167.
11. S.A. Morrow et al. // *Phys. Rev.* 2006, v.C73, p.044611.
12. J. Brudvik et al. // *Summary of the MAX-lab Run Period 2008.04.14 - 2008.04.28.*
13. D. Babusci et al. // *Nucl. Phys.* 1998, v.A 633, p.683.
14. K.-H. Krause et al. // *Nucl. Phys.* 1992, v.A 549, p.387-406.
15. M.P. De Pascale et al. // *Phys. Rev.* 1985, v.C32, p.1830.
16. B. Weissman and H.L. Schultz, // *Nucl.Phys.* 1971, v.A1, p.74-129.
17. E. Whalin, B. Dwight Schriever, A. Hanson // *Phys.Rev.* 1956, v.101, p.377-384.
18. K. Mori et al. // *Phys.Rev.* 1995, v.C51, p.2611.
19. J.l. Matthews et al. // *Nucl. Phys.* 1968, v.A112, p.654.
20. S.V. Springham et al. // *Nucl. Phys.* 1990, v.A517, p.93.
21. J. Ryckebusch et al. // *Phys. Rev.* 1992, v,C46, p.R829.
22. W. Del Bianco et al. // *Phys. Rev. Lett.* 1981, v.47, p.1118.
23. V.P. Barannik, V.G. Gorbenko, V.A. Guschin, et al.// *Yad. Fiz.* 1983, v.38, p.1108 (in Russian).
24. I.E. Vnukov, I.V. Glavanakov, Yu. F. Crechetov, et al.// *Yad. Fiz.* 1988, v.47, p.913 (in Russian).
25. J. Yokokawa et al. // *Journal of the Physical Socirty of Japan.* 1988, v.57, p.695; *NIM.* 1986, v.A 248, p.429.

Appendix

Table 1. *The differential cross section of the $^{12}C(\gamma,p_0)^{11}B$, $^{12}C(\vec{\gamma},p_1)^{11}B$ and the $^{12}C(\gamma,p_{2-6})^{11}B$ reactions for proton emission angle $\theta_p = 85^0$, averaged over all Runs and the targets measurements*

E_γ, MeV	Ground State		$E_{ex} = 2.12$ MeV		$5+7$ MeV	
	$d\sigma/d\Omega$, $\mu b/sr$	Stat.error, $\mu b/sr$	$d\sigma/d\Omega$, $\mu b/sr$	Stat.error, $\mu b/sr$	$d\sigma/d\Omega$, $\mu b/sr$	Stat.error, $\mu b/sr$
41.2	61.01	1.12	15.89	1.35	-	-
45.1	44.60	0.52	11.16	0.83	20.33	0.79
49.0	32.00	0.38	9.79	0.41	20.36	0.79
52.8	23.09	0.38	6.83	0.43	15.63	0.80
56.5	16.55	0.32	4.54	0.32	11.56	0.52
60.2	13.21	0.35	3.83	0.36	9.68	0.51
64.0	9.31	0.34	1.69	0.37	8.79	0.60
67.4	6.80	0.32	1.84	0.43	6.41	0.55
70.8	4.82	0.27	1.34	0.50	6.53	0.50
74.2	3.30	0.27	1.62	0.45	4.11	0.45

Table 2. *The cross section asymmetry of the* $^{12}C(\vec{\gamma}, p_{01})^{11}B$, $^{12}C(\vec{\gamma}, p_{2-6})^{11}B$, $^{12}C(\vec{\gamma}, p_0)^{11}B$ *and* $^{12}C(\vec{\gamma}, p_1)^{11}B$ *reactions averaged over Runs and targets,* $\theta_p = 85^0$

E_γ, MeV	(γ, p_{01})		(γ, p_{2-6})		(γ, p_0)		(γ, p_1)	
	Asymmetry	*Error*	*Asymmetry*	*Error*	*Asymmetry*	*Error*	*Asymmetry*	*Error*
41.2	0.84	0.16	-	-	0.95	0.13	0.47	0.58
45.1	0.87	0.09	0.63	0.20	0.87	0.06	0.53	0.32
49.0	0.83	0.08	0.63	0.17	0.90	0.05	0.64	0.17
52.8	0.74	0.12	0.52	0.31	0.67	0.09	0.90	0.26

АСИММЕТРИЯ СЕЧЕНИЯ $^{12}C(\vec{\gamma}, p_0)^{11}B$ И $^{12}C(\vec{\gamma}, p_1)^{11}B$ РЕАКЦИЙ ПРИ ЭНЕРГИИ ФОТОНОВ 40...55 МэВ

Д.Д. Бурдейный, J. Brudvik, В.Б. Ганенко, K. Hansen, K. Fissum, K. Livingston, L. Isaksson, M. Lundin, B. Nilsson, B. Schröder

Асимметрия сечения $^{12}C(\vec{\gamma}, p_0)^{11}B$ и $^{12}C(\vec{\gamma}, p_1)^{11}B$ реакций была измерена на пучке линейно поляризованных меченных фотонов на MAX-лаб установке в интервале энергий 40...55 МэВ. Показано, что асимметрия процесса $^{12}C(\vec{\gamma}, p_0)^{11}B$ равна $\Sigma \approx 0,85$, что соответствует одночастичному механизму реакции. Асимметрия сечения реакции $^{12}C(\vec{\gamma}, p_1)^{11}B$ меньше, $\Sigma \approx 0,6...0,7$, что может быть связано с более сильным относительным вкладом механизма 2h-1p в доминирующий одночастичный механизм реакции.

АСИМЕТРІЯ ПЕРЕРІЗУ $^{12}C(\vec{\gamma}, p_0)^{11}B$ І $^{12}C(\vec{\gamma}, p_1)^{11}B$ РЕАКЦІЙ ПРИ ЕНЕРГІЯХ ФОТОНІВ 40...55 МеВ

Д.Д. Бурдейний, J. Brudvik, В.Б. Ганенко, K. Hansen, K. Fissum, K. Livingston, L. Isaksson, M. Lundin, B. Nilsson, B. Schröder

Асиметрія перерізу $^{12}C(\vec{\gamma}, p_0)^{11}B$ і $^{12}C(\vec{\gamma}, p_1)^{11}B$ реакцій була виміряна на пучку лінійно поляризованих мічених фотонів на MAX-лаб установці в інтервалі енергій 40...55 МеВ. Показано, що асиметрія процесу $^{12}C(\vec{\gamma}, p_0)^{11}B$ дорівнює $\Sigma \approx 0,85$, що вказує на одночастковий механізм реакції. Асиметрія перерізу реакції $^{12}C(\vec{\gamma}, p_1)^{11}B$ менше, $\Sigma \approx 0,6...0,7$, що може бути пов'язано з більш сильним відносним внеском механізма 2h-1p у домінуючий одночастковий механізм реакції.